Materials Letters 325 (2022) 132799

Contents lists available at ScienceDirect

Materials Letters

journal homepage: www.elsevier.com/locate/matlet

Improved solar water splitting performance of $BiVO_4$ photoanode by the synergistic effect of Zr-Mo co-doping and FeOOH Co-catalyst layer

Maged N. Shaddad [a], Mahmoud Hezam [b,*], Prabhakarn Arunachalam [a,*], Norah M. AL-Saeedan [a], Sixto Gimenez [c], Juan Bisquert [c], Abdullah M. Al-Mayouf [a,d,*]

[a] Electrochemical Sciences Research Chair (ESRC), Chemistry Department, College of Science, King Saud University, Riyadh 11451, Saudi Arabia
[b] King Abdullah Institute for Nanotechnology, King Saud University, Riyadh 11451, Saudi Arabia
[c] Institute of Advanced Materials (INAM), Universitat Jaume I, 12006 Castelló, Spain
[d] K.A.CARE Energy Research and Innovation Center at Riyadh, Saudi Arabia

ARTICLE INFO

Keywords:
Composite materials
Semiconductors
$BiVO_4$
Electrical properties
Co-doping

ABSTRACT

In this work, Zr-Mo co-doping was successfully employed on electrochemically deposited $BiVO_4$ photoanodes, and tested for photoelectrochemical (PEC) water oxidation. Zr doping induced the formation of relatively smaller morphological features resulting in improved light absorption and PEC activity. Mo doping resulted in structural damage that enhanced the charge carrier separation and increased free carrier density. The synergetic effect of both dopants resulted in ~5-fold enhancement of the PEC performance. When a FeOOH layer is hydrothermally grown on the Zr-Mo co-doped $BiVO_4$ electrode, the photocurrent density was enhanced by ~13-fold achieving 3.34 mA/cm^2 at 1.23 V_{RHE}. In addition, the onset potential was remarkably reduced from ~0.45 V to <0.1 V.

1. Introduction

Monoclinic bismuth vanadate (m-$BiVO_4$) is a stable, nontoxic, visible light-absorbing material (bandgap ~ 2.4 eV) with suitable energy band alignment for water oxidation, making it promising for economical solar water splitting [1]. However, the high carrier recombination rate, slow water oxidation kinetics, and photocorrosion are major intrinsic problems to be overcome. Interestingly, it can be resolved by adding an oxygen evolution co-catalyst that simultaneously improves interfacial charge transfer and electrode photo-stability [2–6]. Besides, metal doping has been an efficient strategy to improve electrode performance, although the origin is unclear and can vary from one metal to the other. Mo-doped $BiVO_4$ is one of the successful metal doping approaches reported in the literature [7–9]. Co-doping with two metals at the same time is also reported by many groups; namely Mo/W [10], Mo/Zn [11], and Mo/F [12] have all been described. We recently showed that Zr doping of m-$BiVO_4$ reduces the overall resistance and enhances PEC activity [2,3,13]. Herein, Zr-Mo co-doping results in 5-fold photocurrent density enhancement and their mechanism(s) are discussed for each dopant. Furthermore, with the addition of a FeOOH co-catalyst, the photocurrent was boosted to 3.34 mA/cm^2 and the onset potential was reduced to < 0.1 V.

2. Experimental

A pure, Zr-doped, Mo-doped, and Zr-Mo-doped m-$BiVO_4$ electrodes were electrodeposited with Zr/Bi and Mo/Bi molar ratios of 2.5%. Another Zr-Mo doped electrode was coated with iron oxyhydroxide (β-FeOOH) layer (Fig. S1). The fabricated electrodes were described by X-Ray Diffraction (XRD), FE-SEM, and X-Ray Photoelectron Spectroscopy (XPS). Current density–voltage (J-V), electrochemical impedance spectroscopy (EIS), and IPCE measurements were performed on electrodes, and the details are presented in the supporting information (SI).

3. Results and discussion

Fig. 1**a** shows the XRD pattern of the prepared samples. All samples showed the m-$BiVO_4$ structure (JPCD No. 014–0688) with no additional peaks. This can be explained by the slight doping (2.5%) implemented in our work [14,15]. Zr doping is reported to induce higher texturing along the (1 2 1) direction [10], which can also be observed by the higher (−1 2 1) peak with Zr doping that increases with the Zr concentration up

* Corresponding authors at: Electrochemical Sciences Research Chair (ESRC), Chemistry Department, College of Science, King Saud University, Riyadh 11451, Saudi Arabia (P. Arunachalam and A.M. Al-Mayouf). King Abdullah Institute for Nanotechnology, King Saud University, Riyadh 11451, Saudi Arabia (M. Hezam).
E-mail addresses: mhezam@ksu.edu.sa (M. Hezam), parunachalam@ksu.edu.sa (P. Arunachalam), amayouf@ksu.edu.sa (A.M. Al-Mayouf).

https://doi.org/10.1016/j.matlet.2022.132799
Received 21 March 2022; Received in revised form 17 June 2022; Accepted 4 July 2022
Available online 7 July 2022

to 2.5 mol % (Fig. S2). Besides, Mo-doping degraded the crystallinity of the resulting film in general for both the Mo-doped and the Mo/Zr doped electrodes. Mo-doping is reported to induce such structural degradations to the m-$BiVO_4$ lattice, which can, under low doping levels, be advantageous in enhancing the charge separation (μ_{sep}) efficiency [9,10]. FE-SEM images (Fig. S3) show no appreciable changes between electrodes. However, the Zr-doped sample has relatively smaller grain features than the others. Interestingly, Zr acts as a grain growth inhibitor, as demonstrated earlier for numerous metallurgical synthetic approaches [16]. Fig. 1**b** displays the UV–vis absorption spectra. The absorption onset is not appreciably changed by both dopants. However, Zr doping shows (whether alone or with Mo) a relatively higher above-bandgap absorption (Fig. S4). This might be explained by the relatively smaller grain features, which enhance beneficial light scattering within the m-$BiVO_4$ film. Despite this apparently insignificant doping effect on the structural and optical properties of electrodes, the impact on the PEC performance was remarkable. Fig. 1**c** displays the J-V plots of the prepared electrodes. Doping with Zr alone resulted in a photocurrent improvement from 0.259 mA/cm^2 for bare-$BiVO_4$ to ~ 0.5 mA/cm^2, without a noticeable improvement of the onset potential (Table S1). Mo-doping resulted in an outstanding ~ 3-fold enhancement of the photocurrent to ~ 0.82 mA/cm^2 and reduced the onset potential by ~ 60 mV. Zr-Mo doping resulted in a 5-fold enhancement in photocurrent (~1.26 mA/cm^2), while further reducing the onset potential to ~ 0.3 V. Further, obtained photocurrents are higher than the recently reported $BiVO_4$ photoanodes (Table S2). Fig. S5 discusses the front and back illumination of fabricated electrodes. Fig. 1**d** demonstrates the plots of the ABPE with respect to the applied bias. Also, compared to $BiVO_4$, more than 8-fold enhancements in ABPE was observed after Zr-Mo dopants. Further, the obtained photocurrents were compared to those obtained with a hole scavenger (HS), and the μ_{sep} and charge injection (μ_{inj}) efficiencies were accordingly calculated (Fig. 1**e**). Interestingly, μ_{inj} was increased by both dopants while μ_{sep} was only increased by Mo-doping. The structural degradation induced by Mo-doping can lead to local electric fields that can enhance the separation of the photogenerated carriers to the m-$BiVO_4$ lattice [9,10]. μ_{inj} was therefore synergistically enhanced by both improved μ_{sep} and increased carrier density for the Mo-doped electrodes. Besides, the Zr-doped electrode showed enhanced μ_{inj} merely due to the reduced morphological dimensions induced by Zr-doping. Notably, this reduction is possibly responsible for the slightly enhanced absorption. Additionally, it reduces the length required for holes to reach the water interface, thus directly enhancing μ_{inj}. These results are consistent with the resulting IPCE spectra (Fig. 1**f**), where Mo-doping generates higher spectral photocurrents than Zr-doping, despite the opposite UV–vis absorption behavior. Therefore, Zr and Mo have different routes in enhancing photocatalytic activity.

The effect of individual dopants was explored by XPS. Fig. 2 displays the XPS results of all elemental regions of the Zr-Mo co-doped $BiVO_4$ electrode. The Bi $4f_{7/2}$ peak at 158.8 eV and the V $2p_{3/2}$ peak at 516.6 eV are respectively attributed to the Bi^{3+} and V^{5+} oxidation states [17]. The O 1 s peak could be de-convoluted into two Gaussian peaks at 529.7 eV and 531.1 eV attributed respectively to oxygen in the m-$BiVO_4$ lattice [17] and to surface contaminations. The Zr $3d_{5/2}$ peak could be de-convoluted into two noticeably separated peaks at 181.5 eV and 184.4 eV. We attribute the 181.5 eV peak to the Zr^{3+} in the $BiVO_4$ lattice, while the 184.4 eV peak is attributed to ZrO_2 that we previously reported on the surface Zr-doped $BiVO_4$ electrodes [2,13]. The Mo $3d_{5/2}$

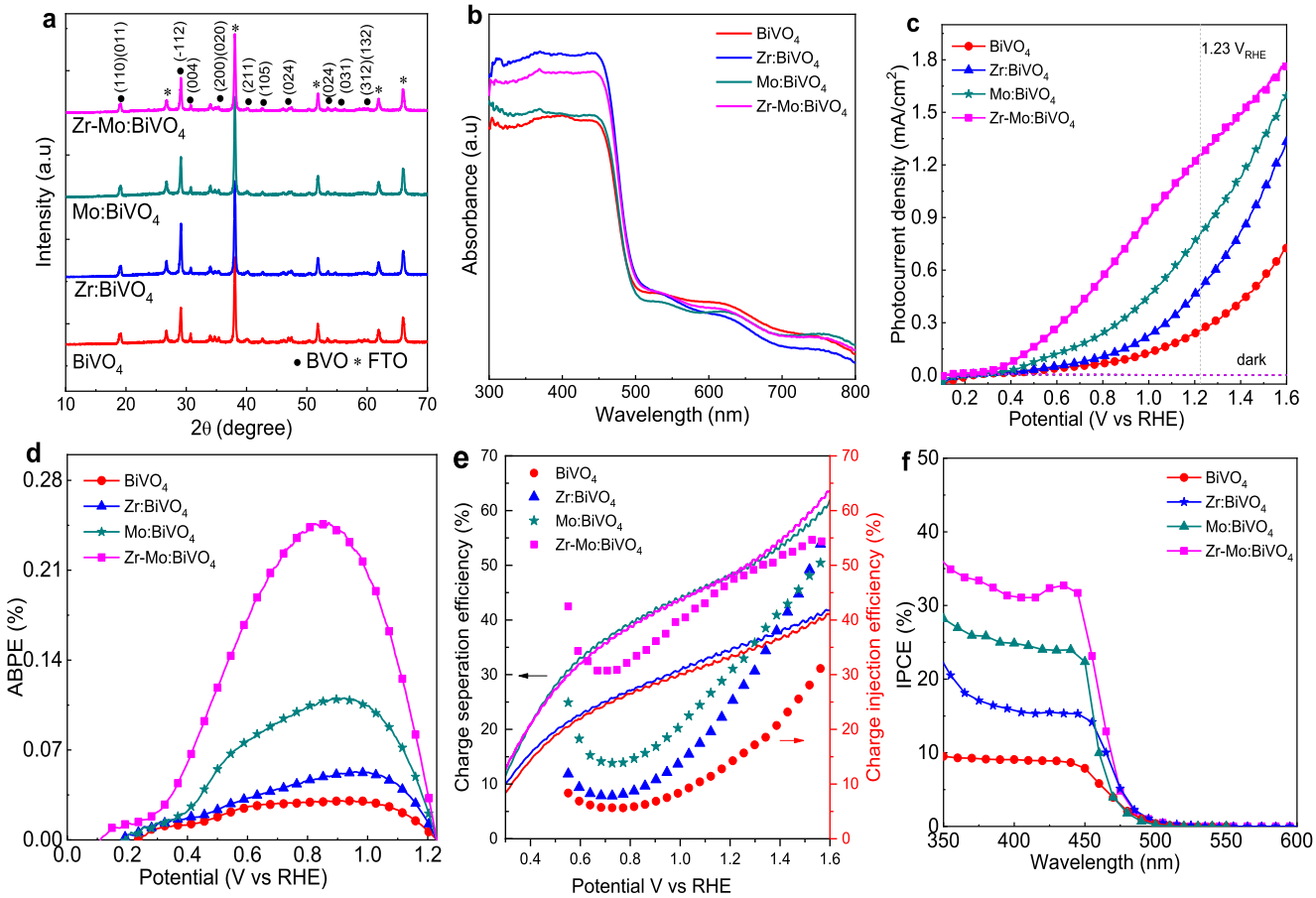

Fig. 1. (a) XRD, (b) UV–vis absorption, (c) J-V curves, (d) ABPE, (e) charge separation and injection efficiencies, and (f) IPCE measurements of fabricated electrodes.

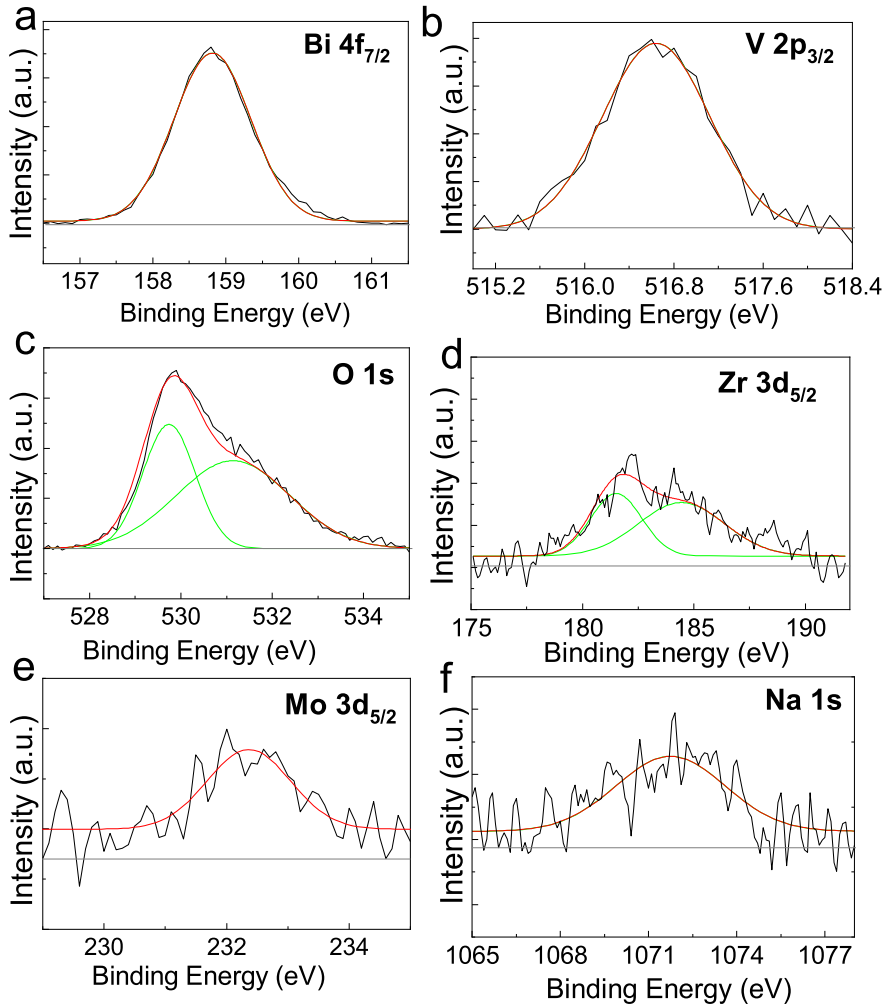

Fig. 2. XPS measurements of Zr-Mo:$BiVO_4$ electrodes.

exhibited a single peak at 232.4 eV, corresponding to the Mo^{6+} oxidation state. Therefore, the doping process can be described as Zr^{3+} replacing the Bi^{3+} ions, and Mo^{6+} replacing the V^{5+} ions, in agreement with increased carrier density by Mo^{6+} doping. It must be noted that Na 1 s was also detected, showing a peak at 1071.7 eV, which can be attributed to unreacted Na_2MoO_4 [18] during electrode fabrication (see SI). Na^+ has a large ionic radius [19], and, therefore less likely to contribute to the doping process in the m-$BiVO_4$ lattice.

The long-term stability of fabricated electrodes was relatively assessed in phosphate buffer and shown in Fig. 3**a**. The Zr-Mo dual-doped films revealed a considerable photocurrent density of ~ 1.28 mA/cm^2, superior to other photoanodes, and there was certainly no apparent decay in the photocurrent, demonstrating their significant long-term stability. Moreover, the observed enhancement can be explained by an improved carrier transport in the doped electrodes. Fig. 3**b** shows the Nyquist plots of electrodes, which agree with the J-V behaviors. Zr doping resulted in a reduced charge transfer resistance, recognized by its smaller arc diameter, further reduced with Mo doping, and was the lowest for the Zr-Mo co-doped electrode (Table S3). Further, from the Mott-Schottky analysis (Fig. 3**c**), the carrier density was calculated, and the values are shown in Table S1. The carrier density increase due to Zr doping is small and indeed within experimental error. Therefore, Zr doping was effectively not increasing the carrier concentration. Notably, Mo-doping increased the free carrier density, supporting the J-V behavior of Mo-doped electrodes.

Finally, when a FeOOH was decorated over Zr-Mo co-doped $BiVO_4$, a 13-fold enhancement was obtained, achieving 3.34 mA/cm^2 (Fig. 3**d**). Compared to the pure $BiVO_4$ electrode, the FeOOH/Zr-Mo:$BiVO_4$ electrode displays a significant cathodic shift of onset potential (~390 mV) (Fig. S6). Also, compared to Zr-Mo:$BiVO_4$, nearly 4-fold enhancements in ABPE were observed after decorating with FeOOH (Fig. S7). The obtained photocurrent is even higher than obtained with a HS for the FeOOH untreated co-doped electrode, reflecting the efficiency of the FeOOH co-catalyst. Lastly, the onset potential was remarkably reduced from ~ 0.45 V for the pure electrode to < 0.1 V for the FeOOH treated Zr-Mo doped electrode.

4. Conclusions

In summary, we developed an optimized $BiVO_4$ electrode in which Zr-Mo co-doping was successfully used to synergistically improve the PEC performance. Mo-doping increased carrier concentration and enhanced charge carrier separation, while Zr doping induced smaller morphological features to enhance the hole collection. FeOOH co-catalyst added to the Zr-Mo-doped electrode boosted the photocurrent by 13-fold and remarkably reduced the onset potential to below 0.1 V.

Declaration of Competing Interest

The authors declare that they have no known competing financial

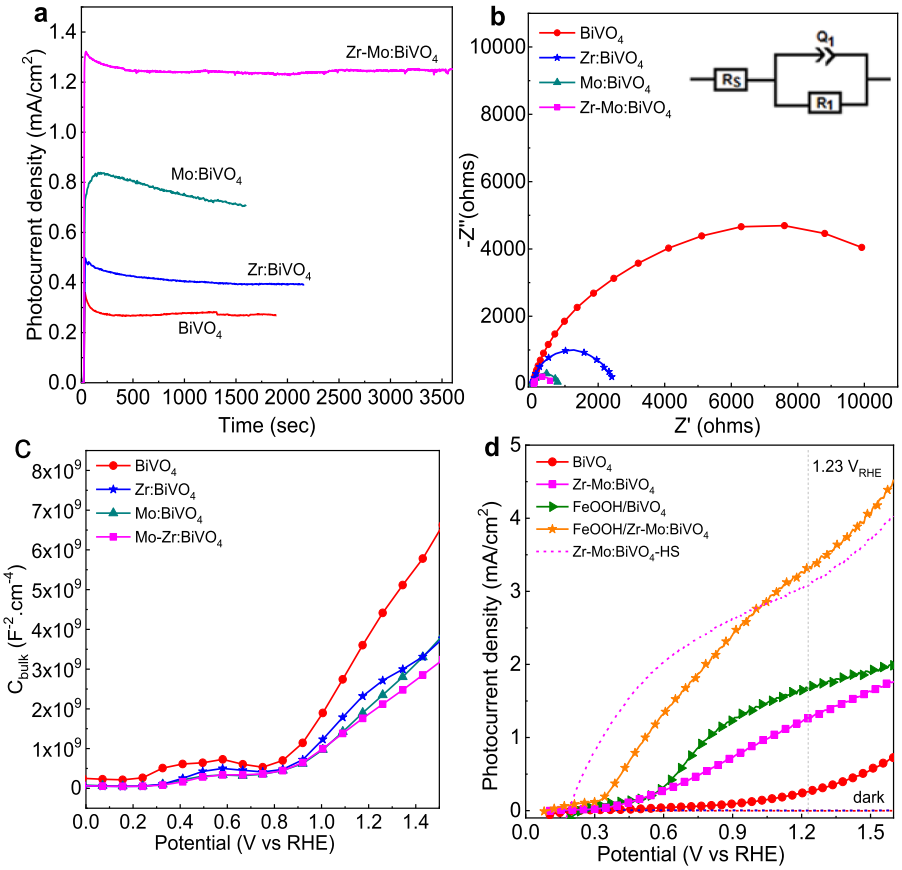

Fig. 3. J-t curves (a), Nyquist plot (b), Mott-schottky plots (c), J-V curves (d) of the bare $BiVO_4$, $FeOOH/BiVO_4$, Zr-Mo:$BiVO_4$, and FeOOH treated Zr-Mo: $BiVO_4$ electrodes.

interests or personal relationships that could have appeared to influence the work reported in this paper.

Acknowledgements

This research was funded by the National Plan for Science, Technology and Innovation (MAARIFAH), King Abdulaziz City for Science and Technology, Kingdom of Saudi Arabia, Award Number (14-ENE2323-02).

Appendix A. Supplementary data

Supplementary data to this article can be found online at https://doi.org/10.1016/j.matlet.2022.132799.

References

[1] Z. Wang, X. Huang, X. Wang, Catal. Today. 335 (2019) 31–38.
[2] M.N. Shaddad, P. Arunachalam, et al., J. Catal. (2019) 10–19.
[3] M.N. Shaddad, P. Arunachalam, et al., Appl. Catal. B Environ. (2019) 863–870.
[4] T. Palaniselvam, L. Shi, et al., Adv. Mater. Interfaces 4 (2017) 1700540.
[5] L. Shi, S. Zhuo, et al., RSC Adv. 8 (2018) 29179.
[6] X. Chang, T. Wang, J. Am. Chem. Soc. 137 (2015) 8356.
[7] S.K. Pilli, T.E. Furtak, L.D. Brown, T.G. Deutsch, J.A. Turner, A.M. Herring, Energy Environ. Sci. 4 (2011) 5028–5034.
[8] M. Rohloff, B. Anke, S. Zhang, U. Gernert, C. Scheu, M. Lerch, A. Fischer, Sustain Energy Fuels. 1 (2017) 1830–1846.
[9] J.A. Seabold, K. Zhu, N.R. Neale, Phys. Chem. Chem. Phys. 16 (2014) 1121–1131.
[10] J.S. Ma, L.Y. Lin, Y.S. Chen, Int. J. Hydrogen Energy. 44 (2019) 7905–7914.
[11] Y. Qian, J. Feng, et al., ACS Appl. Mater. Interfaces. 12 (2020) 16662–16669.
[12] M. Rohloff, B. Anke, O. Kasian, S. Zhang, M. Lerch, C. Scheu, A. Fischer, ACS Appl. Mater. Interfaces. 11 (2019) 16430–16442.
[13] M.N. Shaddad, M.A. Ghanem, A.M. Al-Mayouf, S. Gimenez, J. Bisquert, I. Herraiz-Cardona, ChemSusChem. 9 (2016) 2779–2783.
[14] B. Liu, et al., Materials 10 (2017) 976.
[15] M. Tayebi, A. Tayyebi, B.K. Lee, Catal. Today. 328 (2019) 35–42.
[16] K. He, T.N. Baker, Mater. Sci. Eng. A 256 (1998) 111–119.
[17] P. Chatchai, Y. Murakami, S. ya Kishioka, A.Y. Nosaka, Y. Nosaka, Electrochim. Acta. 54 (2009) 1147–1152.
[18] A. V. Naumkin, A. Kraut-Vass, S.W. Gaarenstroom, C.J. Powell, NIST X-Ray Photoelectron Spectrosc. Database, Version 4.1. (2012).
[19] R.D. Shannon, Acta Crystallogr. Sect. A. 32 (1976) 751–767.